

MsFEM upscaling for the coupled thermo-mechanical problem^{*}

Marek Klimczak¹[0000-0003-2662-9555] and Witold Cecot¹[0000-0002-3257-5226]

Cracow University of Technology, Faculty of Civil Engineering, Poland
mklimczak@L5.pk.edu.pl, plcecot@cyf-kr.edu.pl

Abstract. In this paper, we present the framework for the multiscale thermoelastic analysis of composites. Asphalt concrete (AC) was selected to demonstrate the applicability of the proposed approach. It is due to the observed high dependence of this material performance on the thermal effects. The insight into the microscale behavior is upscaled to the macroresolution by the multiscale finite element method (MsFEM) that has not been used so far for coupled problems. In the paper, we present a brief description of this approach together with its new application to coupled thermoelastic numerical modeling. The upscaled results are compared with the reference ones and the error analysis is presented. A very good agreement between these two solutions was obtained. Simultaneously, a large reduction of the degrees of freedom can be observed for the MsFEM solution. The number of degrees of freedom was reduced by 3 orders of magnitude introducing an additional approximation error of only about 6%. We also present the convergence of the method with the increasing approximation order at the macroresolution. Finally, we demonstrate the impact of the thermal effects on the displacements in the analyzed asphalt concrete sample.

Keywords: Multiscale finite element method · Upscaling · Thermoelasticity · Asphalt concrete.

1 Introduction

The placement of our research, divided into two parts, is presented in this Section. Firstly, we describe the developed AC material models incorporating the thermal effects. Secondly, we present selected multiscale approaches to the modeling of asphalt concrete. Our study encompasses mainly the effects of the heterogeneous AC structure on its performance. In addition, we account for the heat transfer within this material, which affects the mechanical response.

1.1 Asphalt Concrete

Asphalt concrete (AC) is a typical material used for the flexible or semi-rigid pavement structure layers. In this paper, we use this term to describe the composite made of two main ingredients: the mineral aggregate (90 ÷ 95% w/w, where

^{*} This research was supported by the National Science Center (NCN) under grant UMO-2017/25/B/ST8/02752.

w/w stands for the weight ratio) and the mastic ($5\div 10\%$ w/w). The latter is understood as a mixture of the asphalt binder and a very fine mineral filler.

For the sake of simplicity, we neglect in this study the presence of the air voids, the modifiers and other possible additives since the paper focus is on the multiscale analysis rather than on the materials science. The extension of the presented in this paper framework to other asphalt mix types is possible and it does not affect its routine. The only restriction is the analysis scale, which is the continuum. We cannot directly incorporate e.g. the atomistic scale observations to the whole analysis.

In Poland, the term *asphalt concrete* precisely refers to one of the asphalt mix types, which is characterized by the uniform gradation curve. It means that all particle fractions are represented in the aggregate mix with a similar weight ratio. In this paper, we keep this Polish nomenclature. Some other asphalt mixes include SMA (stone mastic asphalt). The comparison between exemplary gradation curves for AC and SMA is shown in Fig. 1.

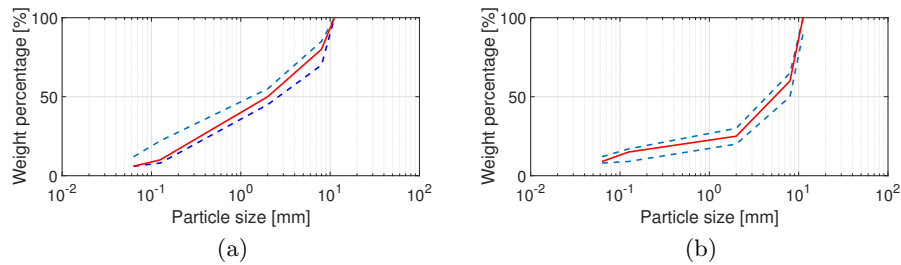


Fig. 1. Exemplary grading curves (red solid line) for (a) AC and (b) SMA - blue dotted lines denote bounding gradation curves according to Polish guidelines

We are able to model any gradation curves. However, in the numerical examples we focus on AC only since its applicability is very broad comparing to other asphalt mix types designed rather for specific pavement layers. Modifying the gradation curve, the asphalt binder content and other properties, AC can be laid for all asphalt pavement layers.

The performance of AC at the continuum scale is based on the mechanisms that can be observed at lower scales. The overview of a number of complex phenomena influencing the overall AC response is presented e.g. in [11,27]. They are related either to external factors such as loading, temperature, aging, moisture, to name only a few, or the internal material structure.

The very basic description of the AC performance is provided by the linear elasticity equations. Namely, all the considered constituents are modeled as linear elastic. In some cases, when the analysis period is very short, the subject load is constant and the temperature is relatively low, such an approach may be sufficient to capture the physical response of AC. Instead of the linear elastic model, more realistic viscoelastic constitutive equations can be easily used. We

have already applied MsFEM for such model [13] but in this paper, we focus on the novel MsFEM implementation, i.e. thermo-mechanical coupling.

In the number of papers, only the aggregate particles are modeled as linear elastic, whereas the asphalt binder is described using a variety of viscoelasticity [24,23,22,29,34], viscoelastoplasticity [18,33] or even more complex models accounting for the accumulated damage [2,12,32]. In some studies, the adhesive (interfacial) zone between the AC constituents is also encompassed in the analysis [19,17,34]. Typically, a perfect bonding between the binder and the aggregate particles, as it is the case in this paper, is assumed.

It should be also remarked that due to the increasing complexity of the above models, not in all of the studies the heterogeneous AC microstructure was considered. Contrary, the effective AC material model was developed.

Temperature, which is considered as one of the major factors influencing the AC performance, is taken into account in a number of studies in several modes. Firstly, the temperature distribution in AC can be regarded as a standalone problem [9,26,31]. Its solution can be used in further specific analyses.

In this paper, we use the so-called *sequential coupling of thermal-stress analysis*. It is a basic approach to the solution of the thermoelasticity problem that is weakly coupled, i.e. the displacement and stress fields are temperature-dependent without the reverse relationship. This algorithm is implemented e.g. in ABAQUS. Since its common application (c.f. [30]), including this study, it is recapitulated below (Algorithm 1). When solving the final elasticity problem, the thermal strain is applied in a form of a contribution to the right-hand side of the governing differential equation.

Algorithm 1 Solve a sequentially coupled thermoelasticity problem

Require: define the problem (geometry, material parameters and boundary conditions)

Ensure: the FE mesh complying with the material distribution

 solve the heat transfer problem within the domain

for $n=1$ to N_{GP} **do** {loop over Gauss points}

 compute the thermal strains resulting from the temperature distribution

 set material parameters for the computed temperature

end for

 solve the elasticity problem with thermal strains and temperature-dependent material parameters

In the *fully coupled thermal-stress analysis*, the displacement/stress fields are computed simultaneously with the temperature field. It is used for the strongly coupled fields affecting each other, contrary to the weakly coupled fields analyzed using the sequential thermal-stress approach according to Algorithm 1. In order to solve such a problem, the multiscale finite element method can be also used.

1.2 Multiscale AC Analyses

As it was mentioned in the previous chapter, the complexity of the AC material models considerably limits their application to the analysis with the heterogeneous microstructure considered. Therefore, homogenized AC effective responses are needed in practice.

The multiscale modeling, that we use in this study, incorporates the information from the lower scale (or scales) to the actual analysis scale. The main goal of these approaches is to transfer this information effectively. Namely, we want to reduce the computation cost by introducing as little additional modeling error as possible.

A number of homogenization and upscaling techniques were developed for the AC modeling [8,11,12,15,20,23,22,28]. Most of them are variants of the FE² homogenization presented in [6]. This approach consists in a two-scale analysis using the finite element method at each level. At the macroscale Gauss points, auxiliary boundary value problems (BVP) are solved to account for the underlying microstructure. The domain used for a single BVP is called the representative volume element (RVE) and should be constructed precisely to reveal the AC microstructure. The advantage of the FE² homogenization is that no material model needs to be used at the macroscale. Instead, the effective quantity Q is passed from RVE using the averaging over the RVE volume V :

$$\langle Q \rangle = \frac{1}{V} \int_V Q dv \quad (1)$$

In [28], the proper orthogonal decomposition (POD) was used to reduce the problem order for the elastic AC computations. These two above-mentioned approaches were combined in [8].

The effective values of the complex modulus and phase angle of the analyzed AC specimen were obtained in [21] using the Generalized Self Consistent Scheme - an analytical model of the idealized inclusion embedded in a matrix.

Due to a number of its advantages, the FE² approach is the most popular. However, its limitation is the distinct separation of scales condition. In the context of the AC numerical modeling, it can be a caveat for the thinner asphalt layers. Namely, the upper pavement layers - wearing and binding course.

The upscaling approach, called the multiscale finite element method (Ms-FEM), was used in [14,15] by us to model the elastic and viscoelastic response of AC. A short description of MsFEM is provided hereinafter.

The upscaled/homogenized solutions for AC modeled as the thermoelastic material are not very common in the literature. General approaches, as in [3,10,25], are rather developed.

To our best knowledge, MsFEM has never been used for such a problem. Thus, the present study aims to fill this gap, demonstrate the initial results and perspectives for further research.

2 Problem Formulation

In this study, we search for the solution of the weakly coupled thermoelasticity problem in a heterogeneous domain using the set of equations recapitulated below. For the sake of simplicity, we do not assume the time-dependency of any of the present fields. As far as the mechanical AC response is considered, the linear elasticity model is used. The temperature distribution is obtained solving the steady-state heat transfer problem. The numerical computations are performed according to Algorithm 1.

Find the displacements $\mathbf{u}(\mathbf{x})$ and the temperature $\Theta(\mathbf{x})$ such that

$$\left\{ \begin{array}{ll} \mathbf{div}\boldsymbol{\sigma} + \mathbf{X} = \mathbf{0} & \forall \mathbf{x} \in \omega_i \subset \Omega \\ \boldsymbol{\sigma} = \mathbf{C}^{-1}[\boldsymbol{\varepsilon}(\mathbf{u}) - \boldsymbol{\varepsilon}^*] & \forall \mathbf{x} \in \omega_i \subset \Omega \\ \boldsymbol{\varepsilon} = \frac{1}{2}[\nabla\mathbf{u} + (\nabla\mathbf{u})^T] & \forall \mathbf{x} \in \omega_i \subset \Omega \\ -k\Delta\Theta = f & \forall \mathbf{x} \in \omega_i \subset \Omega \\ \boldsymbol{\varepsilon}^* = \alpha\mathbf{I}\Theta & \forall \mathbf{x} \in \omega_i \subset \Omega \\ + \text{boundary \& continuity or debonding conditions} & \end{array} \right. \quad (2)$$

where $\boldsymbol{\sigma}$ denotes the stress tensor, \mathbf{X} are the body forces, \mathbf{C} is the tensor of material parameters for elasticity, k is the thermal conductivity, α is the coefficient of thermal expansion and $\boldsymbol{\varepsilon}^*$ is the thermal strain tensor.

Eqs. 2_{IV,V}, referring solely to the heat transfer problem, are solved first. Then, the thermal strains $\boldsymbol{\varepsilon}^*$ are transferred to the mechanical part contributing to the right-hand side of Eq. 2_I. The weak formulation of the mechanical part, used for the finite element computations, is presented below.

Find the displacements $\mathbf{u}(\mathbf{x}, t) \in H_0^1(\Omega) + \hat{\mathbf{u}}$ such that

$$\int_{\Omega} \boldsymbol{\varepsilon}(\mathbf{v}) : \mathbf{C}^{-1}\boldsymbol{\varepsilon}(\mathbf{u})d\omega = \int_{\Omega} \mathbf{v} \cdot \mathbf{X}d\omega + \int_{S_\sigma} \mathbf{v} \cdot \hat{\mathbf{t}}ds + \int_{\Omega} \boldsymbol{\varepsilon}(\mathbf{v}) : \mathbf{C}^{-1}\boldsymbol{\varepsilon}^*d\omega \quad \forall \mathbf{v} \in H_0^1(\Omega) \quad (3)$$

where \mathbf{v} denotes test functions, $\hat{\mathbf{t}}$ are the known tractions, $\hat{\mathbf{u}}$ are the known displacements and H_0^1 is the Sobolev space of the functions satisfying homogeneous Dirichlet boundary conditions.

3 Multiscale Finite Element Method

MsFEM [4,5,7] is one of the upscaling methods. It enables to model the problem at the macroresolution incorporating the lower resolution information. The core of its idea is presented schematically in Fig. 2.

Firstly, regardless of the information on the microstructure, we discretize the domain with the coarse mesh (blue quadrilateral elements in Fig. 2). Then, we proceed element-wise. A fine mesh complying with the microstructure is generated within a given coarse element. Assembly within this subdomain delivers a

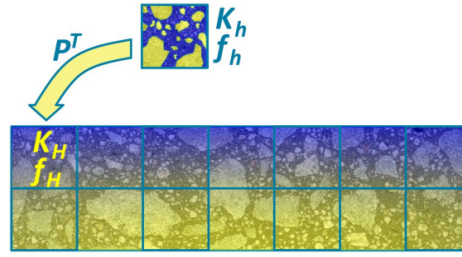


Fig. 2. MsFEM scheme illustrated for a single coarse element

fine mesh stiffness matrix \mathbf{K}_h and a load vector \mathbf{f}_h . Its effective counterparts are computed using the following formulas:

$$\begin{aligned} \mathbf{K}_H &= \mathbf{P}^T \mathbf{K}_h \mathbf{P} \\ \mathbf{f}_H &= \mathbf{P}^T \mathbf{f}_h \end{aligned} \quad (4)$$

Therein, matrix \mathbf{P} stands for the prolongation operator. Its assessment requires the solution to the auxiliary boundary value problem that is used for the search of the modified coarse element shape functions. The degrees of freedom (dof) of the solution for a given shape function constitute the corresponding column of \mathbf{P} .

In the case of the thermoelasticity problem, we need to solve two sets of auxiliary BVP: for the elasticity and the heat transfer problems consequently. For the detailed description of the BVP leading to the assessment of the modified shape functions for the elasticity, we refer to our previous papers [14,15]. For the sake of brevity, only the auxiliary BVP for the heat transfer is presented below.

Given Ψ_m , which is a coarse mesh standard scalar-valued shape function ($m=1, \dots, M$), we look for its scalar-valued counterpart Φ_m that is a discrete solution of the following Dirichlet boundary value problem

$$\begin{cases} \frac{\partial}{\partial x_i} \left(k \frac{\partial \Phi_m}{\partial x_i} \right) = -k^\alpha \frac{\partial^2 \Psi_m}{\partial x_i^2} \quad \forall i=1,2,3, \mathbf{x} \in \Omega_s^j \subset \Omega_s \subset \Omega \\ \Phi_m = \hat{\Phi}_m \quad \text{on} \quad \partial\Omega_s \\ + \text{interface continuity conditions} \end{cases} \quad (5)$$

where k is the thermal conductivity of the material at a given location \mathbf{x} , k^α is the arbitrary averaged thermal conductivity in Ω_s , Ω_s^j denotes the j -th constituent of the composite.

Problem 5 is solved using FEM, thus the corresponding variational formulation needs to be stated. For the completeness of the problem statement, we refer to the comprehensive discussion on the definition of the Dirichlet boundary conditions for Φ_m in [14,15].

Illustration of the MsFEM routine is shown on a simple example of the 1D bar. Let us consider a prismatic bar with a length of 2. Its left half is characterized with $EA=1$, the right one with $EA=10$. Using 2 linear finite elements, their

stiffness matrices are equal to \mathbf{K}_L and \mathbf{K}_R , respectively. Their assembly gives \mathbf{K}_h . Computation of the effective matrix \mathbf{K}_H for one linear coarse element (occupying the whole bar) requires solutions to the corresponding auxiliary problems (see [1]) to obtain prolongation operator \mathbf{P} , consequently. The above-mentioned matrices are given below:

$$\mathbf{K}_L = \begin{bmatrix} 1 & -1 \\ -1 & 1 \end{bmatrix}, \mathbf{K}_R = \begin{bmatrix} 10 & -10 \\ -10 & 10 \end{bmatrix}, \mathbf{K}_h = \begin{bmatrix} 1 & -1 & 0 \\ -1 & 11 & -10 \\ 0 & -10 & 10 \end{bmatrix}, \mathbf{P} = \begin{bmatrix} 1 & 0 \\ 0.09 & 0.91 \\ 0 & 1 \end{bmatrix},$$

$$\mathbf{K}_H = \begin{bmatrix} 0.91 & -0.91 \\ -0.91 & 0.91 \end{bmatrix}.$$

4 Numerical Results

The proposed approach is illustrated with the numerical results for the idealized AC specimen of dimensions 8 cm×20 cm. Material distribution for the arbitrary gradation curve is shown in Fig. 3. As shown in Fig. 3 a, the whole upper edge is subject to heating with $q=30\text{W/m}$, whereas temperature along the bottom edge is equal to 20°C. The remaining edges are insulated. As far as the mechanical part is concerned, the bottom edge is fixed and the load of intensity $t = 100\text{kN/m}$ is subject to the upper edge centrally for 1/5 of its length. Remaining edges are free.

Respective material parameters are presented in Tab. 1. We neglect the change in the Young modulus for the aggregate particles as a function of temperature but we do account for this, crucial in the case of the mastic, phenomenon. We use the Young modulus value measured at temperature 20°C for the pure linear elastic case (see Fig. 6) and another value measured at temperature 50°C. This temperature is approximately equal to the result of the heat transfer problem analyzed in Section 4.1. One can observe a dramatic decrease of the mastic Young modulus value at this temperature. It is two orders of magnitudes smaller than the value at the reference temperature (20°C). For the sake of simplicity, we use only one value of the Young modulus for the whole matrix in the second step of the sequentially coupled thermal-stress analysis. Practically, it is a function of the temperature distribution obtained in the first step (see Fig. 4) and it changes also spatially.

4.1 The thermal part

In the sequentially coupled thermal-stress analysis, the first step is to solve the heat transfer problem. The temperature and thermal strain distribution is shown in Fig. 4. Since all non-zero thermal strain tensor components are equal, we present only one of them.

As it can be observed, the discrepancies between the reference fine mesh solution and the upscaled one are extremely small. The reference solution was obtained using more than 113 000 degrees of freedom (about 220 000 finite elements) and the linear approximation was used. The upscaled solution was

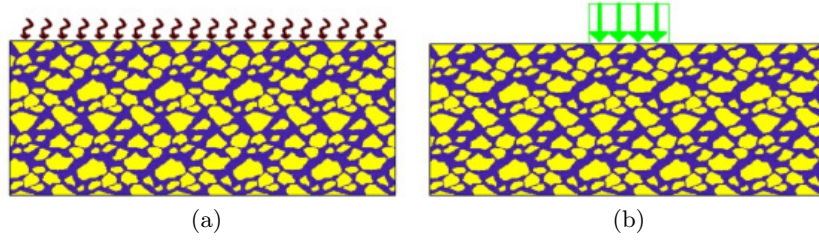


Fig. 3. Neumann boundary conditions for (a) heat transfer and (b) mechanical part

Table 1. Material parameters

Parameter	Unit	Value
Young modulus - inclusion	Pa	80e9
Young modulus - matrix (at 20°C)	Pa	10e9
Young modulus - matrix (at 50°C)	Pa	10e7
Poisson ratio - inclusion	-	0.3
Poisson ratio - matrix	-	0.3
thermal conductivity - inclusion	W/(mK)	0.8
thermal conductivity - matrix	W/(mK)	4.2
coefficient of linear thermal expansion - inclusion	$10^{-6}/^{\circ}\text{C}$	8
coefficient of linear thermal expansion - matrix	$10^{-6}/^{\circ}\text{C}$	190

obtained for a regular mesh of 2×5 coarse elements with the increasing approximation orders ($p=1 \div 5$). The convergence of the temperature and the thermal strain errors measured in L_2 norm is shown in Fig. 5 using the logarithmic scale.

Increasing the approximation order, we observe the reduction of the L_2 error norm for this problem. It drops from about 1.4% (strain) or 1.5% (temperature) for 18 dof to about 1% (both fields) for about 300 dof (instead of about 113 000 fine mesh dof used for the reference solution). This behavior needs a short discussion. Whereas the p -convergence observed at the macroscale is a typical property of many upscaling methods, it can be observed rather for the primary field (temperature for this problem). It is not very common for other fields, derived from the primary one. Thus, this p -convergence observed for both present fields can be regarded as the MsFEM advantage. Thermal strain tensor is a linear function of temperature. However, coefficients of thermal expansion for the matrix (asphalt mastic) and inclusions (mineral aggregate) are significantly different (see Tab. 1). Obtaining such satisfactory results could be cumbersome for a number of upscaling methods. Such a good performance of MsFEM is possible due to the reversible relationship between macro- and microscale degrees of freedom. Thus, after obtaining macroscale ones, we can easily compute in the post-processing also the microscale degrees of freedom and proceed with this more detailed information.

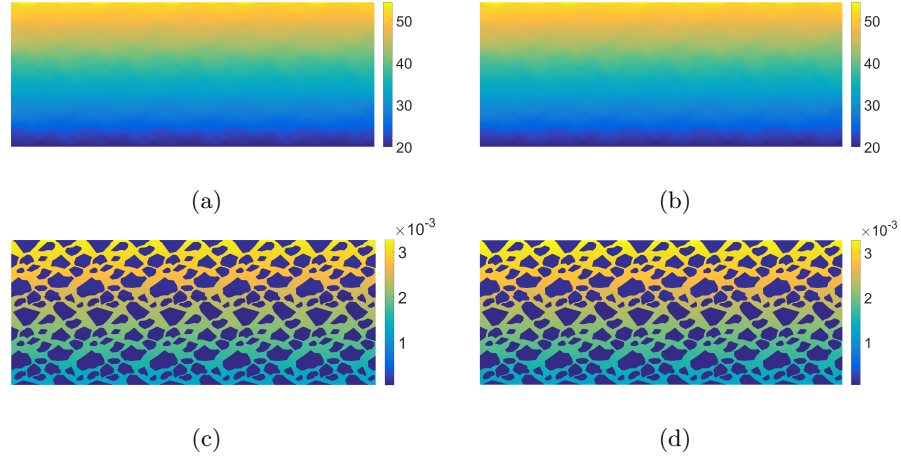


Fig. 4. Maps of temperature (a÷b) and thermal strain (c÷d) - the left column shows the upscaled solution (for $p=5$) and the right one shows the reference fine mesh solution

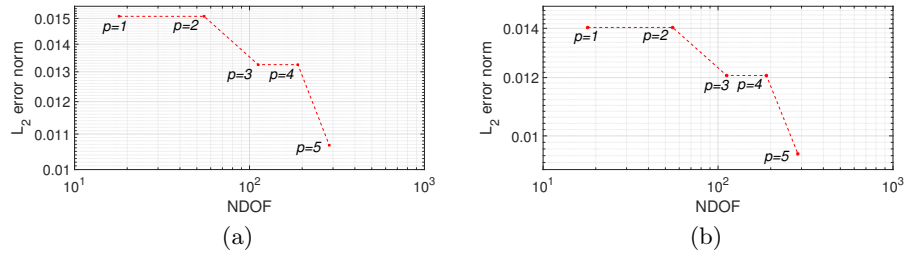


Fig. 5. Error convergence for (a) temperature and (b) thermal strain

Reduction of degrees of freedom compared to the reference fine mesh solution spans from about 6300 ($p=1$) to about 400 ($p=5$) times with the corresponding temperature error values ranging from about 1% ($p=5$) to about 1.5% ($p=1$).

4.2 The mechanical part

The results of the elastic analysis are shown in Fig. 6. We used for this case material parameters for temperature equal to 20°C for the mastic (matrix). A very good agreement between the reference and upscaled solutions can be observed. The p -convergence (Fig. 7) shown both for the L_2 and energy norms demonstrates the benefits of the higher order approximation used at the macroscale. Increasing the approximation order, we reduce the errors measured in L_2 and energy norms from about 20% to about 6% and from about 60% to about 20%, respectively. The corresponding reduction of the fine mesh reference solution de-

degrees of freedom (about 220 000) spans from 18 ($p=1$) to 572 ($p=5$) degrees of freedom.

In Fig. 7 (c÷d), one can observe also the error convergence measured in the same norms with respect to the relative time, i.e. the ratio of the computational time necessary for the upscaled and reference solutions. It demonstrates the applicability of the MsFEM. The time used for the auxiliary problem solution is the price of the method. Thus, the observed speed-up is not as spectacular as the reduction of the NDOF compared to the reference fine mesh solution. The speed-up of about 40 times was obtained in this test for $p=5$ with the corresponding error norms equal to about 6% (L_2 norm) or 20% (energy norm). For a more detailed discussion on the MsFEM computational efficiency, we refer the reader to [13,15]. Some crucial aspects of the discussion presented therein are:

- MsFEM is ready for the parallelization, the auxiliary problems can be solved independently
- formally cumbersome computations (associated with the auxiliary problems repeated for every standard shape function) reduce to the system of the algebraic equations with multiple right-hand sides
- locally assembled fine mesh stiffness matrix \mathbf{K}_h used in 4_I can be directly taken from the local auxiliary problem, no additional computational effort is necessary.

It should be remarked that the overall MsFEM computational efficiency depends mostly on the implementation, the problem being solved and the discretization at both scales. The obtained speed-up can be, thus, different at various applications.

The results of the linear elastic analysis are presented to illustrate subsequently the effect of the heat transfer within the AC sample on its overall response. The presented results are used for the forthcoming comparative study.

In the second step of the sequentially coupled thermal-stress analysis, i.e. the mechanical part, we use the temperature distribution obtained at the first step in a twofold manner. Firstly, we modify the material parameters according to the temperature distribution (in this study, we used the same parameters for the whole domain). Secondly, we compute the thermal strains according to the formula 2 v and use them to contribute to the right-hand side as presented in Eq. 3. The final results (displacements) are presented in Fig. 8. The error norms are approximately equal to those presented for the linear elastic case, which can be considered as the MsFEM advantage.

A short discussion on the accuracy of the results presented in this section is necessary. Firstly, the error convergence presented in Fig. 5 and 7 does not support strongly the idea of the higher order approximation. Particularly, in Fig. 5, the results obtained for the higher p are very similar to those for $p=1$. It is due to a relatively smooth solution that can be efficiently captured using only the linear approximation at the macroscale. In our previous papers [1,13,15,14], we demonstrated a number of results in favor of the higher order approximation. Secondly, further improvement of the MsFEM accuracy can be obtained using

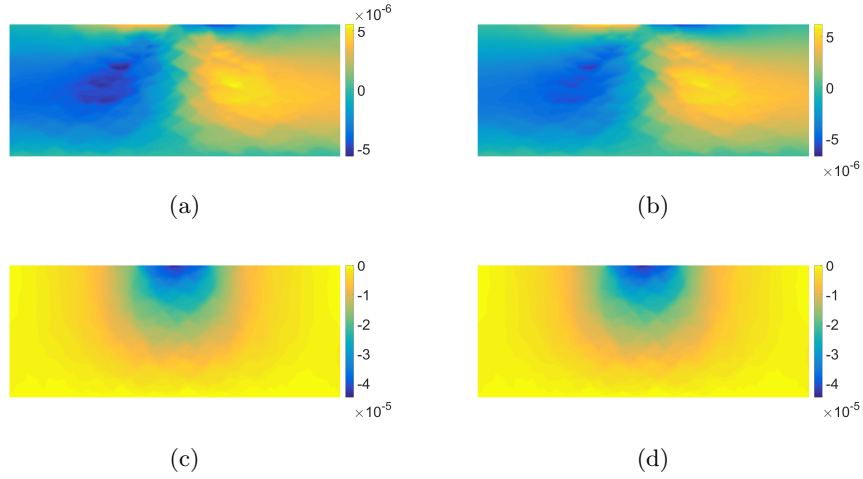


Fig. 6. Displacement maps: (a÷b) u_x component and (c÷d) u_y component - the left column shows the upscaled solution (for $p=5$) and the right one shows the reference fine mesh solution

e.g. error estimates based on the residual, which is the topic of our forthcoming paper. Using this approach, a significantly better p -convergence can be observed.

Comparing the results presented in Figs. 6 and 8, one can observe a large modification in the AC sample response. Firstly, both of the displacement components increased substantially. Secondly, due to the applied heating, the horizontal displacements approximately equaled with the vertical ones up to the order of magnitude. Thirdly, the predominant vertical displacement of the upper edge reflects a very common failure of the asphalt pavement structure (or the wearing course solely). Namely, the rut is observed together with the bulged neighborhood. The upscaled solution captures this response almost as precisely as the reference one but with the large reduction of the degrees of freedom.

5 Concluding remarks

In the paper, we presented a novel approach to upscaling for the coupled thermoelastic modeling of composites. The framework was tested on the example of asphalt concrete. However, it is general and not limited to the materials of a similar class. Our previous studies [1,13,16] refer also to other kinds of heterogeneous materials. Herein, we combined the well-known sequentially coupled thermal-stress analysis with the developed version of MsFEM. The convergence error confirmed the benefits of the higher order approximation. Reduction of about 220 00 dof to about 600 introduced modeling error of only about 6%. This error can be further reduced using the hp -adaptivity (c.f. [13]) or other ap-

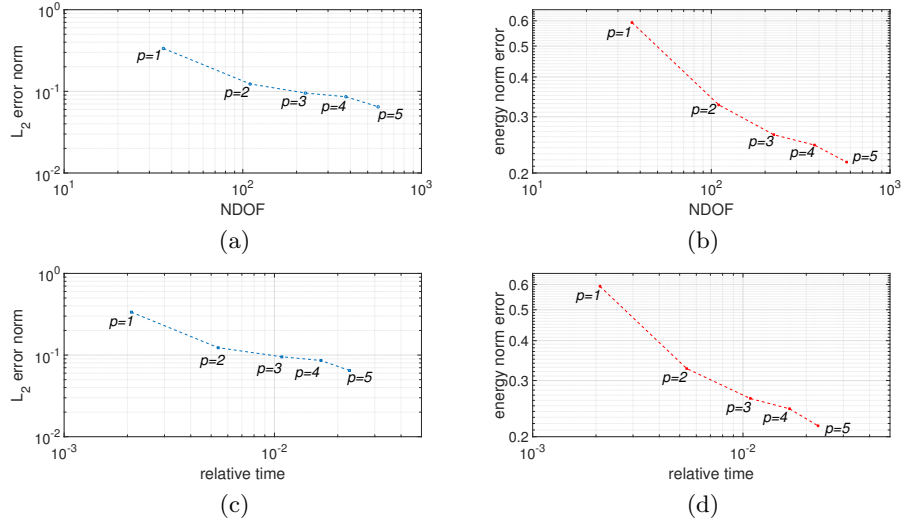


Fig. 7. Error convergence measured in (a) L_2 norm and (b) energy norm with respect to NDOF and the same convergence types (c÷d) with respect to the relative time (by the relative time, we mean the ratio of the computational time necessary for the upscaled and the reference fine mesh solutions)

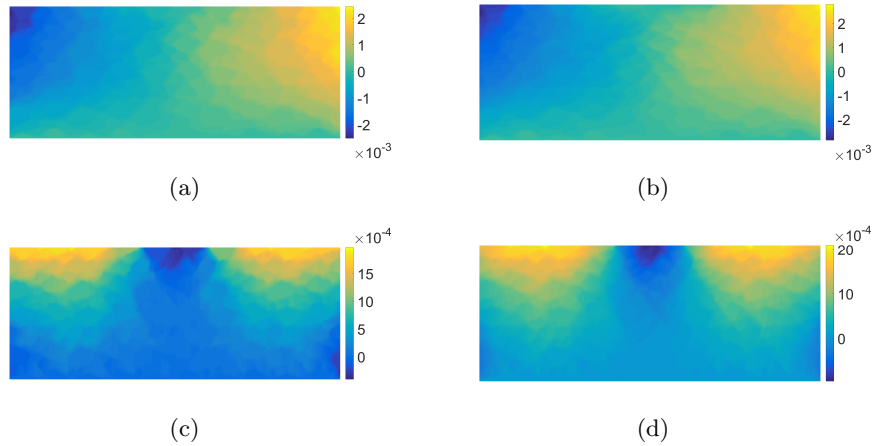


Fig. 8. Displacement maps: (a÷b) u_x component and (c÷d) u_y component - the left column shows the upscaled solution (for $p=5$) and the right one shows the reference fine mesh solution

proaches. To our best knowledge, MsFEM with the higher order shape functions has never been used previously for the thermoelastic analysis.

Our further research effort is to apply this framework to the unsteady heat transfer problem and thermoviscoelastic analysis of asphalt concrete. This can be very useful in the reliable modeling of flexible pavement structures.

References

1. Cecot, W., Oleksy, M.: High order FEM for multigrid homogenization. *Computers and Mathematics with Applications* **70**(7), 1391–1400 (2015)
2. Collop, A., Scarpas, A., Kasbergen, C., de Bondt, A.: Development and finite element implementation of a stress dependent elasto-visco-plastic constitutive model with damage for asphalt. *Transportation Research Record* **1832**, 96–104 (2003)
3. Eden, M., Muntean, A.: Homogenization of a fully coupled thermoelasticity problem for a highly heterogeneous medium with a priori known phase transformations. *Mathematical Methods in the Applied Sciences* **40** (2017)
4. Efendiev, Y., Hou, T.: Multiscale finite element methods for porous media flows and their applications. *Applied Numerical Mathematics* **57**, 577–596 (2007)
5. Efendiev, Y., Hou, T.: *Multiscale Finite Element Methods*. Springer (2009)
6. Feyel, F., Chaboche, L.: FE^2 multiscale approach for modelling the elasto-viscoplastic behaviour of long fibre SiC/Ti composite materials. *Computer Methods in Applied Mechanics and Engineering* **183**, 309–330 (2000)
7. Hou, T., Wu, X.: A multiscale finite element method for elliptic problems in composite materials and porous media. *Journal of Computational Physics* **134**, 169–189 (1997)
8. Jänicke, R., Larsson, F., Runesson, K., Steeb, H.: Numerical identification of a viscoelastic substitute model for heterogeneous poroelastic media by a reduced order homogenization approach. *Computer Methods in Applied Mechanics and Engineering* **298**, 108–120 (2016)
9. Kalluvila, J., Krishnan, A.: Structural and thermal analysis of asphalt solar collector using finite element method. *Journal of Energy* **2014** (2014)
10. Kehrer, L., Wood, J., Böhlke, T.: Mean-field homogenization of thermoelastic material properties of a long fiber-reinforced thermoset and experimental investigation. *Journal of Composite Materials* **54**(25), 3777–3799 (2020)
11. Kim, Y.: *Modeling of Asphalt Concrete*. ASCE Press (2009)
12. Kim, Y., Souza, F., Teixeira, J.: A two-way coupled multiscale model for predicting damage-associated performance of asphaltic roadways. *Computational Mechanics* **51**(2), 187–201 (2013)
13. Klimczak, M., Cecot, W.: An adaptive MsFEM for non periodic viscoelastic composites. *International Journal for Numerical Methods in Engineering* **114**(8), 861–881 (2018)
14. Klimczak, M., Cecot, W.: Synthetic microstructure generation and multiscale analysis of asphalt concrete. *Applied Sciences* **10**(3), 765 (2020)
15. Klimczak, M., Cecot, W.: Towards asphalt concrete modeling by the multiscale finite element method. *Finite Elements in Analysis and Design* **171**, 103367 (2020)
16. Krówczyński, M., Cecot, W.: A fast three-level upscaling for short fiber reinforced composites. *International Journal for Multiscale Computational Engineering* **15**(1), 19–34 (2017)
17. Liu, P., Hu, J., Wang, D., Oeser, M., Alber, S., Ressel, W., Fala, G.: Modelling and evaluation of aggregate morphology on asphalt compression behavior. *Construction and Building Materials* **133**, 196–208 (2017)

18. Mitra, K., Das, A., Basu, S.: Mechanical behavior of asphalt mix: An experimental and numerical study. *Construction and Building Materials* **27**(1), 545–552 (2012)
19. Mo, L., Huurman, M., Wu, S., Molenaar, A.: 2D and 3D meso-scale finite element models for ravelling analysis of porous asphalt concrete. *Finite Elements in Analysis and Design* **44**(4), 186–196 (2008)
20. Neumann, J., Simon, J.W., Mollenhauer, K., Reese, S.: A framework for 3D synthetic mesoscale models of hot mix asphalt for the finite element method. *Construction and Building Materials* **148**, 857–873 (2017)
21. Sawda, C.E., Fakhari-Tehrani, F., Absi, J., Allou, F., Petit, C.: Multiscale heterogeneous numerical simulation of asphalt mixture. *Material Design & Processing Communications* **1**(3), e42 (2019)
22. Schüller, T., Jänicke, R., Steeb, H.: Nonlinear modeling and computational homogenization of asphalt concrete on the basis of XRCT scans. *Construction and Building Materials* **109**, 96–108 (2016)
23. Schüller, T., Manke, R., Jänicke, R., Radenberg, M., Steeb, H.: Multi-scale modelling of elastic/viscoelastic compounds. *ZAMM - Journal of Applied Mathematics and Mechanics* **93**, 126–137 (2013)
24. Tehrani, F.F., Absi, J., Allou, F., Petit, C.: Heterogeneous numerical modeling of asphalt concrete through use of a biphasic approach: Porous matrix/inclusions. *Computational Materials Science* **69**, 186–196 (2013)
25. Temizer, I., Wriggers, P.: Homogenization in finite thermoelasticity. *Journal of the Mechanics and Physics of Solids* **59**(2), 344–372 (2011)
26. Tu, Y., Li, J., Guan, C.: Heat transfer analysis of asphalt concrete pavement based on snow melting. In: *2010 International Conference on Electrical and Control Engineering*. pp. 3795–3798 (2010)
27. Wang, L.: *Mechanics of Asphalt: Microstructure and Micromechanics*. The McGraw-Hill Companies, Inc (2011)
28. Wimmer, J., Stier, B., Simon, J.W., Reese, S.: Computational homogenisation from a 3D finite element model of asphalt concrete - linear elastic computations. *Finite Elements in Analysis and Design* **110**, 43–57 (2016)
29. Woldekidan, M., Huurman, M., Pronk, A.: Linear and nonlinear viscoelastic analysis of bituminous mortar. *Transportation Research Record: Journal of the Transportation Research Board* **2370**(1), 53–62 (2013)
30. Xue-liang, Y., Bo-ying, L.: Coupled-field finite element analysis of thermal stress in asphalt pavement. *Journal of Highway and Transportation Research and Development (English Edition)* **2**(1), 1–6 (2007)
31. Yavuzturk, C., Ksaibati, K., Chiasson, A.: Assessment of temperature fluctuations in asphalt pavements due to thermal environmental conditions using a two-dimensional, transient finite-difference approach. *Journal of Materials in Civil Engineering* **17**(4), 465 (2005)
32. You, T., Al-Rub, R., Darabi, M., Masad, E., Little, D.: Three-dimensional microstructural modeling of asphalt concrete using a unified viscoelastic-viscoplastic-viscodamage model. *Construction and Building Materials* **28**(1), 531–548 (2012)
33. Zbiciak, A.: Constitutive modelling and numerical simulation of dynamic behaviour of asphalt-concrete pavement. *Engineering Transactions* **56**(4), 311–324 (2008)
34. Ziaei-Rad, V., Nouri, N., Ziaei-Rad, S., Abtahi, M.: A numerical study on mechanical performance of asphalt mixture using a meso-scale finite element model. *Finite Elements in Analysis and Design* **57**, 81–91 (2012)